



Full length article



Hydrogen induced structural phase transformation in ScNiSn-based intermetallic hydride characterized by experimental and computational studies

Volodymyr A. Yartys^{a,*}, Vasyl V. Berezovets^{a,1}, Ponniah Vajeeston^b, Lev G. Akselrud^c, Vladimir Antonov^d, Vladimir Fedotov^d, Steffen Klenner^e, Rainer Pöttgen^e, Dmitry Chernyshov^f, Michael Heere^{g,2}, Anatoliy Senyshyn^h, Roman V. Denys^a, Ladislav Havelaⁱ

^a Institute for Energy Technology, P.O. Box 40, Kjeller N-2027, Norway

^b Department of Chemistry, University of Oslo, Oslo N-0315, Norway

^c Max Planck Institute for Chemical Physics of Solids, Nöthnitzer Str. 40, Dresden 01187, Germany

^d Institute of Solid State Physics RAS, Moscow District, Chernogolovka 142432, Russia

^e Institut für Anorganische und Analytische Chemie, Universität Münster, Münster D-48149, Germany

^f SNBL/ESRF, Grenoble Cedex 9, 38043, France

^g Forschungsreaktor München – FRMII, Karlsruhe Institute of Technology, Karlsruhe, Germany

^h Heinz Maier-Leibnitz Zentrum (MLZ), Technical University Munich, Munich-Garching, Germany

ⁱ Charles University, Ke Karlovu 5, Prague 121 16 Czech Republic

ARTICLE INFO

Keywords:

Metal-hydrogen systems
Metal hydride
Neutron powder diffraction
Mössbauer spectroscopy
DFT calculations

ABSTRACT

Understanding an interrelation between the structure, chemical composition and hydrogenation properties of intermetallic hydrides is crucial for the improvement of their hydrogen storage performance. Ability to form the hydrides and to tune the thermodynamics and kinetics of their interaction with hydrogen is related to their chemical composition. Some features of the metal–hydrogen interactions remain however poorly studied, including chemistry of Sc-containing hydrides. ZrNiAl-type ScNiSn-based intermetallic hydride has been probed in the present work using a broad range of experimental techniques including Synchrotron and Neutron Powder Diffraction, ¹¹⁹Sn Mössbauer Spectroscopy, hydrogenation at pressures reaching several kbar H₂ and hydrogen Thermal Desorption Spectroscopy studies. Computational DFT calculations have been furthermore performed. This allowed to establish the mechanism of the phase-structural transformation and electronic structure changes causing a unique contraction of the metal lattice of intermetallic alloy and the formation of the ...H-Ni-H-Ni... chains in the structure with H atoms carrying a partial negative charge. Such hydrogen absorption accompanied by a formation of a covalent Ni-H bonding and causing an unusual behavior contracts to the conventionally observed bonding mechanism of hydrogen in metals as based on the metallic bonding frequently accompanied by a jumping diffusion movement of the inserted H atoms – in contrast to the directional Metal-Hydrogen bonding observed in the present work. At high applied pressures ScNiSnH_{0.83} orthorhombic TiNiSi type hydride is formed with H atoms filling Sc₃Ni tetrahedra. Finally, this study shows that scandium closely resembles the behavior of the heavy rare earth metal holmium.

1. Introduction

Rare earth metals (RE) form equiatomic RENiSn intermetallic

compounds, which crystallize with the orthorhombic TiNiSi type of structures. They form three types of hydrides where in each case hydrogen atoms are accommodated in the tetrahedral RE₃Ni sites,

* Corresponding author.

E-mail address: volodymyr.yartys@ife.no (V.A. Yartys).

¹ Present address: Karpenko Physico-Mechanical Institute, NAS of Ukraine, 5, Naukova Str., Lviv 290601, Ukraine.

² Present address: Technical University of Braunschweig, Institut für Verbrennungskraftmaschinen, Hermann-Blenk-Straße 42, 38108 Braunschweig, Germany.

<https://doi.org/10.1016/j.actamat.2022.118549>

Received 30 August 2022; Received in revised form 17 November 2022; Accepted 20 November 2022

Available online 24 November 2022

1359-6454/© 2022 The Author(s). Published by Elsevier Ltd on behalf of Acta Materialia Inc. This is an open access article under the CC BY license (<http://creativecommons.org/licenses/by/4.0/>).

hexagonal ZrBeSi-type LaNiSnH₂ [1, 2], orthorhombic TiNiSi-type NdNiSnH_{1.0} [3] and hexagonal ZrNiAl-type HoNiSnH_{0.67} [4, 5]. Various types of RENiSn-based hydrides were studied so far and characterized by a variety of techniques, including LaNiSnH_{2.0} [1], CeNiSnH_{1.0} [6] and CeNiSnH_{2.0} [7], PrNiSnH_{1.0} [8], NdNiSnH_{1.0} [3], TbNiSnH_{1.0} [9] and HoNiSnH_{0.67} [4].

Maximum hydrogen storage capacity of RENiSn-based hydrides of 2 atoms H/formula unit is reached in the La and Ce compounds. These hydrides both adopt structures of higher symmetry – hexagonal – while the original intermetallics crystallize with orthorhombic unit cells. The hydrogenation results in filling by hydrogen atoms of all available tetrahedral RE₃Ni sites. In the TiNiSi structure these sites are deformed and contain nonequivalent RE–Ni bond distances while the RE₃Ni tetrahedra become regular with all bonds equivalent on increasing the symmetry to a hexagonal structure. When half of the available RE₃Ni tetrahedra is filled in an ordered way, then the TiNiSi type structure is preserved. However, it becomes significantly internally deformed resulting in a lowering of the symmetry from the centrosymmetric space group *Pnma* to the non-centrosymmetric space group *Pna2₁*. It appears that filling of the RE₃Ni tetrahedra by H atoms is a driving force of the rebuilding of the orthorhombic TiNiSi type HoNiSn structure into a hexagonal ZrNiAl type. During the rebuilding of the structure, the trigonal bipyramidal sites Ho₃Ni₂ are formed with H atoms filling every second of the Ho₃Ni tetrahedra connected by the Ho₃ base. As these tetrahedra are very spacy to accommodate H atoms, a contraction of the lattice ($\Delta V/V = -0.64\%$) takes place. Interestingly, the structure of HoNiSnD_{0.67} is isostructural with the chemically related RENiInD_{0.5–0.6}, formed by La to Nd [10].

The RENiSn based hydrides are all thermally very stable. They reversibly decompose in vacuum above 473 K with one or two decomposition steps and form initial intermetallic alloys. Very unexpectedly, a disproportionation of the intermetallics to form rare earth hydrides has never been observed even though those interstices filled by hydrogen atoms are RE-metal rich and thus should be prone to the separation of rare earths to form the binary REH_{2–3} hydrides.

Scandium, even though not belonging to the lanthanide group of the rare earth metals, resembles properties of the heavy lanthanides. Equiatomic intermetallics ScT₂Sn are formed by many transition metals T (T = Co, Ni, Cu, Pd, Ag, Pt, Au) which crystallize with different structure types. While the structures of ScCoSn [11–13] and ScNiSn [13] belong to the orthorhombic TiNiSi type, ScPdSn [14, 15], ScAgSn [16] and ScPtSn [14, 15] crystallize with structures that are derived from the hexagonal ZrNiAl type. Formation of a particular type of structure is related to the sizes of the atoms of transition metals and valence electrons concentration.

Investigations of hydrogen interaction with Sc-containing intermetallic phases were limited to the studies of the hydrogen interaction with Laves type ScT₂ intermetallics (T = Fe, Co, Ni, Mn) [17–19]. These studies showed that hydrogen storage capacities and thermal stabilities of the Sc-containing Laves type hydrides are lower as compared to the RE-containing analogues. This is most probably caused by the geometrical factors – contraction of the lattice on a replacement of the larger atoms of lanthanide group of rare earth metals (radii between 1.87 Å (La, maximum value) to 1.64 Å (Lu, minimum value)) by scandium with an atomic radius of 1.64 Å [20]. Furthermore, the electronic shell of Sc does not contain *f*-electrons as for the atoms of lanthanide metals, which causes obvious differences in the electronic structures of the compounds of lanthanides and scandium.

This work is the first study where a hydride based on the ternary intermetallic compound of scandium- ScNiSn - has been synthesized and extensively studied using various experimental techniques, including studies of the hydrogenation properties at pressures reaching several kBar H₂ and thermal stability of the formed hydride by using thermal desorption spectroscopy, its characterization using synchrotron X-ray diffraction, neutron powder diffraction, ¹¹⁹Sn Mössbauer spectroscopy and DFT modelling allowing to probe fine details of the metal-hydrogen

interactions.

2. Experimental

2.1. Synthesis of the alloy

The intermetallic compound ScNiSn was prepared using an electric arc furnace by arc melting of the constituent elements (overall purity: Sc – 99.9 wt.%, Ni – 99.99 wt.%, and Sn – 99.999 wt.%) under a purified argon atmosphere. The sample was subsequently annealed at 870 K for 720 hours and then quenched in an ice-water mixture.

2.2. Hydrogenation studies and thermal desorption spectroscopy characterization

The ScNiSn-based hydride has been synthesized in a Sieverts' type experimental setup. The amount of hydrogen absorbed by the material has been determined using a volumetric method by monitoring pressure changes during hydrogen/deuterium absorption in a known volume (accuracy of the measurements 0.1 %). Hydrogen desorption has been studied using thermal desorption spectroscopy (TDS), by heating the sample in a dynamic vacuum in a temperature range 298–923 K when applying a heating rate of 2 K·min⁻¹.

2.3. Synchrotron X-ray diffraction

The high-resolution Synchrotron X-ray powder diffraction measurements were performed at BM31, SNBL, ESRF, France. The monochromatic radiation with a wavelength of 0.31306 Å was used. The samples were sealed in glass capillaries with a diameter of 0.5 mm. ScNiSn: 2 theta range 3.205–30.385°; Step size 0.005°. ScNiSnH_{0.5}: 2 theta range 3.465–30.375°; Step size 0.005°.

2.4. Neutron powder diffraction

Neutron powder diffractometer SPODI at research reactor FRM-II, Munich, Germany [21] has been utilized for the data collection. The wavelength was 1.5482 Å, while in the measurements performed at Oak Ridge National Laboratory, USA [22], the Instrument WAND² has been used (the wavelength was 1.487 Å). 2 theta range 5.5–150.1°; Step size 0.1°.

2.5. Rietveld refinements of the powder diffraction data

The multi-purpose computer software program package WinCSD for crystallographic calculations using powder X-ray and neutron diffraction data has been utilized during the assessment of the SR XRD and NPD data [23].

2.6. High pressure hydrogenation

Two hydrides, ScNiSnH_{0.83} and ScNiSnH_{0.62}, were synthesized under a hydrogen pressure of 2 GPa at ISSP RAS from the initial ScNiSn alloy and from the ScNiSnH_{0.5} sample prepared at IFE, respectively. The samples of ScNiSn and ScNiSnH_{0.5} of about 100 mg each were loaded with hydrogen by a 48 hours exposure to an H₂ pressure of 2 GPa at 373 K followed by their rapid cooling (quenching) to 83 K. The experiments were carried out in a “lentic” type high-pressure chamber [24] using AlH₃ as an internal H₂ source. The hydrogenation method is described in more detail elsewhere [25]. The synthesized samples were ground in an agate mortar under liquid nitrogen and further stored in liquid nitrogen to prevent hydrogen losses. The thermal stability and the hydrogen content of the samples were determined by hot extraction of hydrogen into a pre-evacuated measuring system in the regime of heating from 88 to 853 K at a rate of 10 K·min⁻¹. The mass of the analyzed probe was a few milligrams; the H-to-metal atomic ratio of the probe was estimated

from the pressure of the released gas with a relative accuracy of 5%. The method is described in more detail in [26]. The powdered $\text{ScNiSnH}_{0.83}$ and $\text{ScNiSnH}_{0.62}$ samples were examined by X-ray diffraction at 85 K with a Siemens D500 diffractometer using $\text{Cu-K}\alpha_1$ radiation. The diffractometer was equipped with a custom-designed nitrogen cryostat that permitted loading of the samples without intermediate warming.

2.7. ^{119}Sn Mössbauer spectroscopy

The ^{119}Sn Mössbauer spectroscopic measurements of the ScNiSn and $\text{ScNiSnH}_{0.5}$ samples were conducted with a $\text{Ca}^{119}\text{SnO}_3$ source in usual transmission geometry at 78 K in a commercial nitrogen bath cryostat. The source was kept at room temperature. To reduce the K X-rays emitted by the ^{119}Sn Mössbauer source, a thin palladium foil (thickness 0.05 mm) was placed in front of the detector. The optimized absorber thickness was calculated according to the work of Long et al. [27]. Each sample was placed within a thin-walled PMMA container and was diluted with α -glucose. The WinNormos of Igor6 program package [28] was used to obtain suitable transmission integral fits for the ^{119}Sn spectra.

2.8. Theoretical calculations

Total energies have been calculated by the projected-augmented plane-wave (PAW) implementation of the Vienna ab initio simulation package (VASP) [29, 30]. All these calculations were made using the Perdew, Burke, and Ernzerhof (PBE) [31] exchange-correlation functional. Ground-state geometries were determined by minimizing both the stresses and the Hellman-Feynman forces using the conjugate-gradient algorithm with a force convergence threshold of $10^{-3} \text{ eV}\cdot\text{\AA}^{-1}$. Brillouin zone integration was performed with a Gaussian broadening of 0.1 eV during all relaxations. From various sets of calculations, it was found that 2050 k points in the Brillouin zone for the structure with a 600 eV plane-wave cut-off are sufficient to ensure optimum accuracy in the computed results. The k- points mesh was generated using the Monkhorst-Pack method with a grid size of $10\times 10\times 4$ for structural optimization. Iterative relaxation of atomic positions was stopped when the change in total energy between successive steps was smaller than 1 meV/cell. H atoms partially and with much varying occupancies fill $2d$ (68.6%) and $1a$ (4%) sites in the crystal structure of $\text{ScNiSnH}_{0.5}$. Our theoretical calculations show that the energy difference between these two sites is 0.04 eV and that the $2d$ sites are much higher populated by H atoms as compared to the $1a$ site. Thus, for simplification, in our total energy calculations, we assumed that $2d$ sites are occupied with the 100 % occupancy resulting in the chemical composition $\text{ScNiSnH}_{0.667}$ while at the same time in these calculations we assumed that $1a$ site is empty.

3. Results and discussion

3.1. Synchrotron diffraction study of ScNiSn

The synchrotron radiation diffraction pattern (Supplementary Information, Fig. S1) showed that the precursor sample contains two phases. Its major constituent – 91 wt.% – is the intermetallic compound ScNiSn with TiNiSi type structure (Space group $Pnma$ (No. 62)) and refined unit cell parameters are $a=6.6276(2)$, $b=4.3581(2)$, $c=7.4879(3)$ \AA , $V=216.28(2)$ \AA^3 , while the secondary phase – 9 wt.% – is $\text{ScNi}_{2-x}\text{Sn}$ with a defect Heusler type structure.

Refinement of the SR XRD pattern showed an excellent agreement between the experimental data and calculated diffraction pattern (see Figure S1). The crystallographic data is listed in Table S1.

The crystal structure of ScNiSn of TiNiSi type contains distorted trigonal prisms Sc_6 centered by Ni and Sn thus giving SnSc_6 and NiSc_6 polyhedra. Sn and Ni form a buckled network which can be clearly observed in Fig. 1.

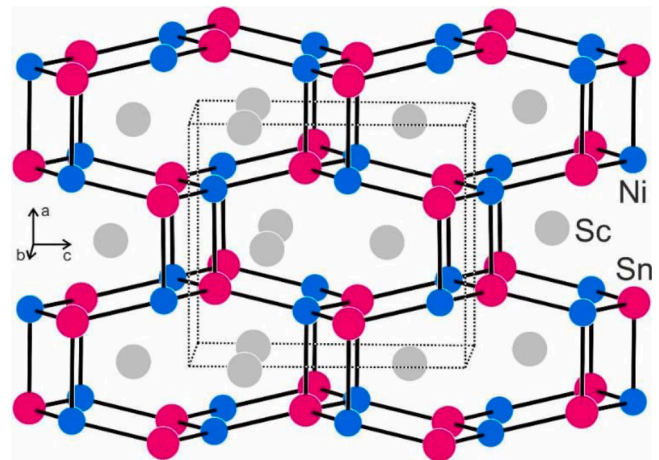


Fig. 1. The structure of ScNiSn (TiNiSi -type, Sp.gr. $Pnma$). The three-dimensional $[\text{NiSn}]$ buckled network is emphasized.

Crystallographic data for the secondary present in the studied alloy intermetallic phase $\text{ScNi}_{2-x}\text{Sn}$ is listed in Table S2 and well agrees with the reference information [32]. This intermetallic crystallizes with Cu_2MnAl type of structure ($a=6.1821(3)$ \AA , $V=236.27(4)$ \AA^3 , $Z=4$; Space group $Fm\bar{3}m$ (No. 225)) and contains defects on Ni sites.

3.2. Synthesis of hydride and studies of its thermal stability

Details of synthesis of $\text{ScNiSnH}_{0.6}$ hydride are given in the Supplementary Information file.

A thermal desorption study showed that the formed hydride contained 0.6 at. H/f.u. ScNiSn . The formed hydride has a high thermal stability with hydrogen desorption occurring in a broad temperature range from 473 to 923 K with two desorption events. The first broad and prolonged peak got a maximum at approximately 723 K and was followed by a sharp peak with a maximum at 873 K (Fig. 2). Hydrogen desorption was complete at temperatures slightly higher than 873 K.

Indexing of the X-ray diffraction pattern showed that the hydride possessed a hexagonal structure with the unit cell parameters $a=7.0555(2)$, $c=3.7414(2)$ \AA . Rietveld profile fitting of the XRD pattern of the formed hydride $\text{ScNiSnH}_{0.5}$ showed that the hydrogenation resulted in a structural phase transformation from an orthorhombic TiNiSi type to a hexagonal ZrNiAl -type.

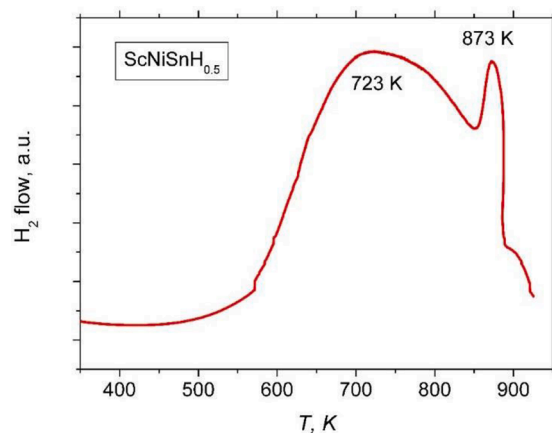


Fig. 2. Hydrogen thermal desorption spectrum of $\text{ScNiSnH}_{0.5}$ measured at a heating rate of 2 K min^{-1} .

3.3. Synchrotron XRD study of the ScNiSnH_{0.5} hydride

Refinements of the synchrotron XRD pattern (Fig. 3a) showed that an insertion derivative to the intermetallic compound ScNiSn – the deuteride ScNiSnH_{0.5} – constitutes a vast majority of the studied sample, 87 wt.%. The hydrogenation/deuteration resulted in a transformation of the TiNiSi type structure of the metal substructure into the hexagonal ZrNiAl type structure with unit cell parameters $a = 7.0555(2)$, $c = 3.7414(2)$ Å, $V = 161.29(2)$ Å³, Sp.gr. *P62m* (No. 189). An unusual and quite significant volume contraction on hydrogenation (by - 0.8 %) took place and is associated with rebuilding of the crystal structure (reconstructive phase transition).

Further to the main phase constituent, the studied sample also contained two minor impurities, including unreacted ScNiSn (TiNiSi-type; 7 wt.%) and a secondary phase admixture of the enriched by nickel ScNi_{2-x}Sn intermetallic compound. Crystal structure data for the deuteride ScNiSnH_{0.5} are listed in Table S3.

The interatomic distances Sc–Sc, Sc–Ni, Sc–Sn and Ni–Sn are presented in the Table S4. All distances with exception of Sc–Sc are close to the sums of the corresponding metallic radii (Sc 1.641 Å; Sn 1.623 Å; Ni 1.246 Å [20]). For Sc–Sc the interatomic distances (3.730 Å) are significantly longer as compared to the doubled atomic radius of Sc, 3.282 Å.

The RENiSn stannides with RE= Sc, Y, La-Nd, Sm, Gd-Lu [33, 34] show high-pressure (11.5 GPa) / high-temperature (T_{\max} up to 1570 K) driven phase transitions from the TiNiSi to the ZrNiAl type structure (multi-anvil cell experiments). In the present work, we have realized this reconstructive phase transition for the metal substructure of ScNiSn through its hydrogenation leading to the hydride ScNiSn_{0.5}.

3.4. Neutron diffraction study of ScNiSnD_{0.5}

Neutron diffraction has been performed using a separately prepared deuterated sample. Deuterium has been used instead of hydrogen to decrease the incoherent scattering of neutrons by the sample and to increase neutron scattering length. The sample contained 85 % of the major phase, ScNiSnD_{0.5} ZrNiAl-type deuteride (85%), which is just marginally smaller as compared to the data of the SR XRD study. The impurities, TiNiSi type orthorhombic ScNiSn and Cu₂MnAl type ScNi_{2-x}Sn, were the same as for the hydride sample studied by SR XRD (Table S5). Further to the metal substructure, the Rietveld refinements (Fig. 3b) allowed to identify the positions of the deuterium atoms in the

structure. The deuterium atoms D1 fill the centers of the trigonal bipyramidal sites Sc₃Ni₂ (Fig. 4). A very small amount of D is also filling the trigonal bipyramidal Sn₃Ni₂ sites occupied by D2.

Since the hydrogenation causes a contraction of the volume, the specific expansion as related to one absorbed H atom cannot be calculated. However, the presence of spacy Sc₃Ni₂ trigonal bipyramids created a large interstitial space in their centers which becomes occupied by H/D atoms. Not surprisingly, the Sc–D and Ni–D bonding distances are relatively large, 2.1531(6) Å and 1.8654(2) Å (see Table S6 for the list of interatomic distances in the structure), respectively which both are close or larger as compared to the values observed earlier for the typical Sc- and Ni- containing ternary hydrides characterized by neutron diffraction - ScFe₂D_{2.5-2.9} [35, 36], LaNiSnD_{2.0} [1], CeNiSnD_{1.0} [6], NdNiSnD_{1.0} [3], HoNiSnD_{0.67} [4] and LaNiD_{3.6} [37].

The crystallographic data of the impurity phases - ScNiSn-based solid solution of D and ScNi_{2-x}Sn ($x = 0.4$) intermetallic are listed in the Tables S2 and S3, respectively.

3.5. High pressure hydride synthesized at 2 GPa H₂

The stannide ScNiSn has been hydrogenated at 2 GPa hydrogen pressure during its heating to 373 K for 48 hours. An XRD study of the quenched to the liquid nitrogen sample showed a formation of a new type of hydride (Fig. 5a). An excellent fit of the diffraction pattern has

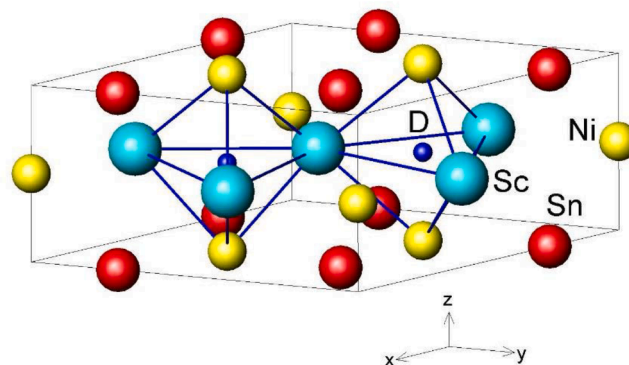


Fig. 4. Crystal structure of ScNiSnD_{0.5} (structure type ZrNiAl). Only the trigonal bipyramidal sites Sc₃Ni₂ occupied by D1 atoms are shown.

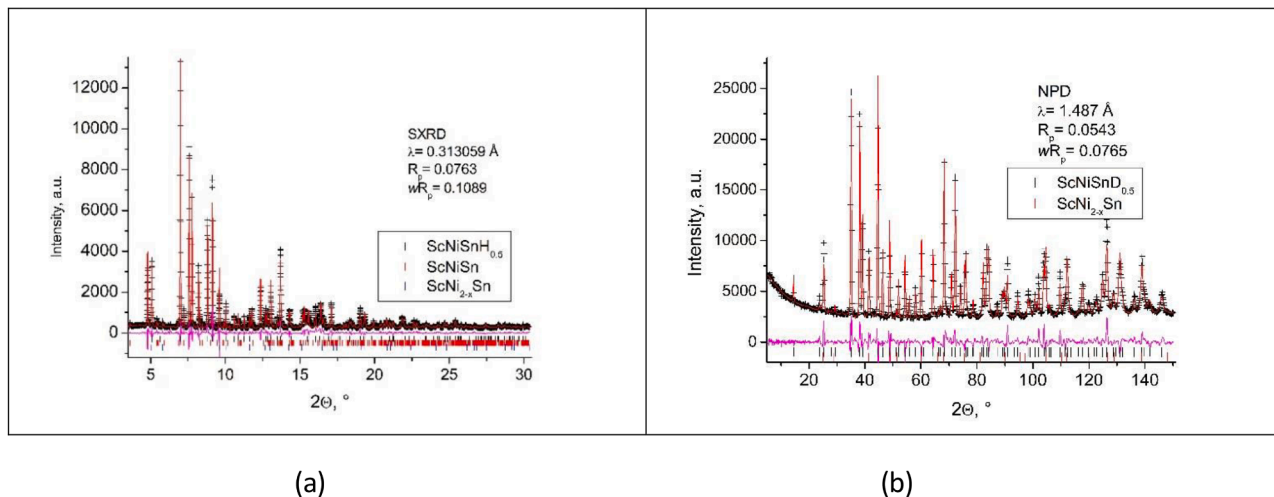


Fig. 3. (a) Rietveld refinement of the synchrotron X-ray powder diffraction pattern measured at 295 K. 2 theta angle range was 3.465-30.375°; Step size 0.005°; $\lambda = 0.313059$ Å. Experimental data: points; calculated data: line; residual intensities plot: bottom line. Positions of the peaks are shown by ticks; ScNiSnH_{0.5} – top; ScNiSn – middle; ScNi_{2-x}Sn – bottom. (b) Rietveld profile fit of the neutron powder diffraction pattern of ScNiSnD_{0.5} ($\lambda = 1.487$ Å) at 295.0 K. Experimental data: points; calculated data: line; residual plot: bottom line. Positions of the peaks are shown by ticks; ScNiSnD_{0.5} – top; ScNi_{2-x}Sn – bottom.

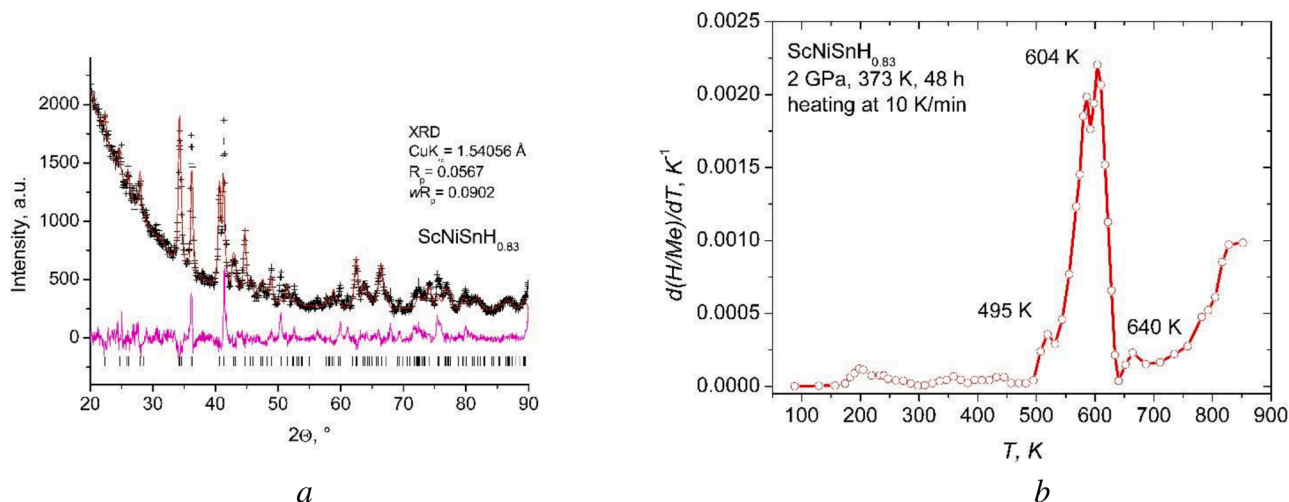


Fig. 5. (a) Rietveld refinements of the XRD pattern (Cu $K_{\alpha 1}$) for the high-pressure hydride $\text{ScNiSnH}_{0.83}$ synthesized by exposing a virgin alloy to 2 GPa H_2 at 373 K for 48 h. (b) Thermal Desorption Spectroscopy spectrum of $\text{ScNiSnH}_{0.83}$ showing that the main desorption event occurs at significantly lower temperature – between 495 and 640 K with a peak at 604 K – as compared to $\text{ScNiSnH}_{0.5}$.

been achieved and is consistent with an orthorhombic TiNiSi type unit cell, $a = 6.830(2)$, $b = 4.056(2)$, $c = 7.967(3)$ Å, $V = 216.28$ Å³. The formation of the hydride results in anisotropic expansion of the initial unit cell, $\Delta a/a = 3.05\%$, $\Delta b/b = -6.91\%$, $\Delta c/c = 6.40\%$. This provides an overall expansion of $\Delta V/V = 2.04\%$.

Thermal desorption spectroscopy performed on heating up to 853 K showed desorption of 0.83 at.H/f.u. ScNiSn (Fig. 5b) with the most pronounced peak of hydrogen desorption occurring at significantly lower temperature – around 604 K – as compared to the hydride synthesized at 10 bar H_2 . Thus, a more extensive hydrogenation has been achieved at high pressures.

Synthesized at hydrogen pressure of 10 bar H_2 at IFE $\text{ScNiSnH}_{0.5}$ (673 K) has been subjected at ISSPh RAS to a hydrogen pressure of 2 GPa at 373 K for 48 hours. Its XRD study (Figure S2) showed the formation of a mixture of the hydride $\text{ScNiSnH}_{0.5}$ with ZrNiAl type structure and a new, more hydrogen-rich hydride phase. A thermal desorption spectroscopy study at temperatures up to 853 K showed that the hydrogen content was 0.62 at.H/f.u. ScNiSn , which indicated an incomplete conversion of $\text{ScNiSnH}_{0.5}$ to the hydride HP- $\text{ScNiSnH}_{0.83}$.

From the comparison of the XRD pattern of $\text{ScNiSnH}_{0.5}$ and $\text{ScNiSnH}_{0.83}$ plotted in Fig. S2 we conclude that a significant rebuilding of the lattice takes place on a formation of a higher $\text{ScNiSnH}_{0.83}$ hydride. Crystallographic data for the high-pressure hydride $\text{ScNiSnH}_{0.83}$ are listed in the Table S7.

The orthorhombic TiNiSi -type structure of $\text{ScNiSnH}_{0.83}$ is shown in Figure 6. Expansion of the structure of ScNiSn creates rather spacy Sc_3Ni interstices with radii of 0.50 Å which are outlined in the Figure 6. These tetrahedra are the most probable sites for the insertion of H atoms. The Sc_3Ni tetrahedra contain long interatomic distances, $\text{Sc-Ni} = 2 \times 2.85$ and 2.92 Å; $\text{Sc-Sc} = 2 \times 3.44$ and 4.06 Å. Large size of these interstices and their surrounding enriched with scandium makes them attractive for the insertion of hydrogen atoms. Filling of all Sc_3Ni sites will result in the formation of the monohydride $\text{ScNiSnH}_{1.0}$ meaning that these tetrahedra are nearly completely occupied by H atoms in the crystal structure of $\text{ScNiSnH}_{0.83}$.

3.6. ^{119}Sn Mössbauer spectra

The ^{119}Sn Mössbauer spectra of the ScNiSn and $\text{ScNiSnH}_{0.5}$ samples recorded at 78 K are presented in Fig. 7a together with transmission integral fits. The corresponding fitting parameters are listed in Table 1. Both spectra could be well reproduced by single signals which were subjected to quadrupole splitting. For ScNiSn the present results are in a

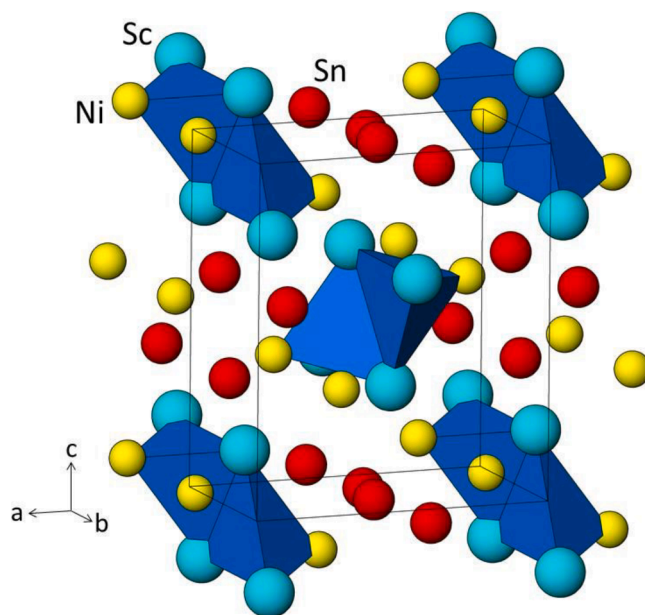


Fig. 6. The crystal structure of $\text{ScNiSnH}_{0.83}$. The outlined Sc_3Ni tetrahedra are the most suitable sites for the accommodation of the hydrogen atom.

good agreement with a previous measurement ($\delta = 1.77(2)$ mm·s⁻¹, $\Delta E_Q = 0.87(2)$ mm·s⁻¹ and $\Gamma = 0.92(4)$ mm·s⁻¹ [38]). Hydrogenation leads to a reconstruction of the metal substructure from the orthorhombic TiNiSi to the hexagonal ZrNiAl type. The near neighbour coordination for the tin atoms in both phases is presented in Fig. 7b. Along with the hydrogenation we observe an increase of the tin site symmetry from m to $m2m$. This higher site symmetry is reflected in a decrease of the quadrupole splitting parameter from $\Delta E_Q = 0.984(1)$ mm·s⁻¹ to 0.714(7) mm·s⁻¹. The isomer shifts of both phases are in the usual range observed for the metal stannides [39]. The slightly lower isomer shift in the hydride indicates slightly lower s electron density at tin nuclei. We note that such a trend is usual in the ^{119}Sn Mössbauer spectroscopy [40]. However, for the presently studied pair $\text{ScNiSn}/\text{ScNiSnH}_{0.5}$ the trends are opposite to the pairs $\text{CeRhSn}/\text{CeRhSnH}_{0.8}$ and $\text{CeIrSn}/\text{CeIrSnH}_{0.7}$ [41], where, in both cases, the hydride shows the higher isomer shift and thus higher electron density at the tin nuclei. Nevertheless, we need to keep in mind, that the cerium-based hydrides keep their ZrNiAl

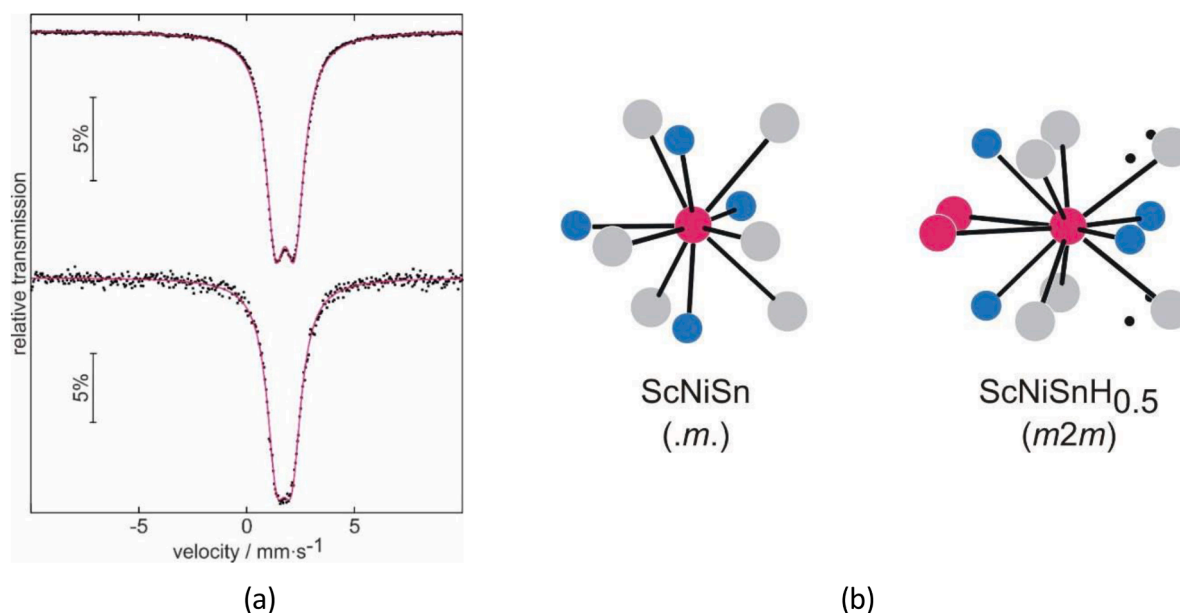


Fig. 7. (a) Experimental (black dots) and simulated (magenta lines) ^{119}Sn Mössbauer spectra of ScNiSn (top) and ScNiSnH_{0.5} (bottom) at 78 K. (b) Coordination of the tin atoms in the structures of ScNiSn and ScNiSnH_{0.5}. Scandium, nickel, tin and hydrogen atoms are drawn in grey, blue, magenta and black color. The hydrogen atoms in the ScNiSnH_{0.5} coordination sphere are drawn for completeness. There are no bonding Sn–H interactions.

Table 1

Fitting parameters of ^{119}Sn Mössbauer spectroscopic measurements at 78 K for ScNiSn and ScNiSnH_{0.5}. δ = isomer shift, ΔE_Q = quadrupole splitting, Γ = experimental line width.

Compound	δ (mm·s ⁻¹)	ΔE_Q (mm·s ⁻¹)	Γ (mm·s ⁻¹)
ScNiSn	1.773(1)	0.984(1)	1.10(1)
ScNiSnH _{0.5}	1.732(3)	0.714(7)	1.07(1)

substructure.

Since the change in isomer shift (and thus in electron density) is small, the charge transfer of the hydrogenation reaction mainly involves the scandium and nickel atoms. This is comparable to the small difference in the ^{121}Sb isomer shift for the pair CeRhSb/CeRhSbH_{0.2} [42].

3.7. Theoretical calculations of the electronic structure of ScNiSnH_{0.667}

For our theoretical study, we have considered ScNiSn and ScNiSnH_{0.667} compounds in both TiNiSi (*Pnma*) and ZrNiAl (*P62m*) type structures. The theoretically obtained unit cell parameters are presented along with experimental data in Table 2. From these tables it is evident that the equilibrium structural parameters obtained from our theoretical calculations are in a very good agreement with the corresponding

Table 2

Crystallographic parameters – experimental and calculated – for ScNiSn and ScNiSnD_{0.5}

	Experimental data (Å)	Theoretical calculations (Å)
ScNiSn	$a = 7.2020$; $c = 3.5328$;	$a = 7.1875$; $c = 3.6056$;
Sp.gr. <i>P62m</i> (No. 189)		
ScNiSn	$V = 52.89 \text{ \AA}^3/\text{f.u. ScNiSn}$	$V = 53.77 \text{ \AA}^3/\text{f.u. ScNiSn}$
Sp.gr. <i>Pnma</i> (No.62)	$a = 6.637$; $b = 4.356$; $c = 7.488$; $V = 54.12 \text{ \AA}^3/\text{f.u. ScNiSn}$	$a = 6.776$; $b = 4.5019$; $c = 7.4398$; $V = 56.74 \text{ \AA}^3/\text{f.u. ScNiSn}$
ScNiSnH _{0.667}	$a = 7.0555$; $c = 3.7414$;	$a = 7.0963$; $c = 3.6712$;
Sp.gr. <i>P62m</i> (No. 189)		
ScNiSnH _{0.667}	$V = 53.76 \text{ \AA}^3/\text{f.u. ScNiSnH}_{0.667}$	$V = 53.36 \text{ \AA}^3/\text{f.u. ScNiSnH}_{0.667}$

experimental findings, differing within just 1.0 % from the experimental values. From the considered for ScNiSn and ScNiSnH_{0.667} compounds structure models, the ZrNiAl-type derived model has the lowest total energy (Fig. 8). This finding is consistent with the experimental studies. However, for ScNiSn compound the energy difference between the Sp.gr. *P62m* and Sp.gr.

Pnma is very small (0.07 eV at the energy curve minimum), and above the unit cell volume of $56 \text{ \AA}^3/\text{f.u.}$ the sp.gr. *Pnma* structure has a lower energy. This clearly indicates that ScNiSn compound may transform to TiNiSi type structure at high temperatures. A similar type of the temperature dependent phase transition has been experimentally observed in Fe_{1+ δ} Se_{0.57}Te_{0.43} [43] and theoretical calculations also reproduce this finding [44]. To further confirm our theoretical predictions, more experimental investigations are in need.

The simulated total density of states (DOS) and electronic band structure at the equilibrium volume for ScNiSn and ScNiSnH_{0.667} in the Sp.gr. *P62m* are displayed in Fig. S3. In these phases, the number of electrons at the Fermi energy $N(E_F)$ is finite, indicating that all studied materials are metallic conductors. Moreover, the up and down spin contributions are equal; thus, both ScNiSn and ScNiSnH_{0.667} show paramagnetic behaviors. The electronic structures of ScNiSn and ScNiSnH_{0.667} are almost similar, except that for the hydride an additional electron density is coming from the extra electrons of the H atoms while $N(E_F)$ in ScNiSnH_{0.667} shifts towards the conduction band (Fig. 9).

The calculated partial DOS of the studied phases in the sp.gr. *P62m* are displayed in Fig. S4. Interestingly, that for both ScNiSn and ScNiSnH_{0.667} compounds, the evident metallic conductivity behavior mainly originates from the contributions from the Sn-*p* and Sc-*d* states.

Due to the different coordination of the Ni(1) and Ni(2) atoms in the structures, their energy levels significantly vary from each other. In ScNiSn, the Ni(1)-*d* states are occupied between -3 to -1.3 eV region, while Ni(2) site *d*-states are occupied between -2.5 to -0.89 eV region. Similarly, in ScNiSnH_{0.667}, for the Ni(1) site the Ni-*d* states are occupied between -3 to -1.3 eV region, while the Ni(2) site *d*-states are occupied between -2.8 to -1.05 eV region. For both compounds, their common feature appears to be in a fact that Sc-*d* (occupied between -4.6 to 0 eV) and Sn-*p* states (occupied between -5.0 to 0 eV) remain unchanged on the hydrogenation.

In the hydrogenated phase the H-*s* states are mainly occupied

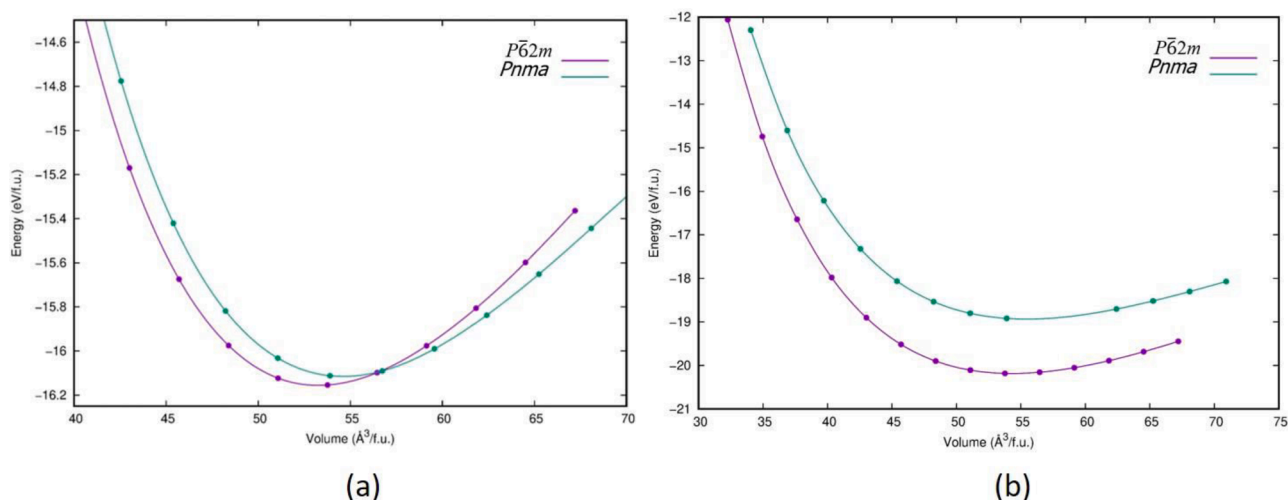


Fig. 8. Calculated total energies as a function of the unit-cell volumes for the hexagonal ZrNiAl- and orthorhombic TiNiSi-type structures of (a) ScNiSn and (b) ScNiSnH_{0.667} hydride.

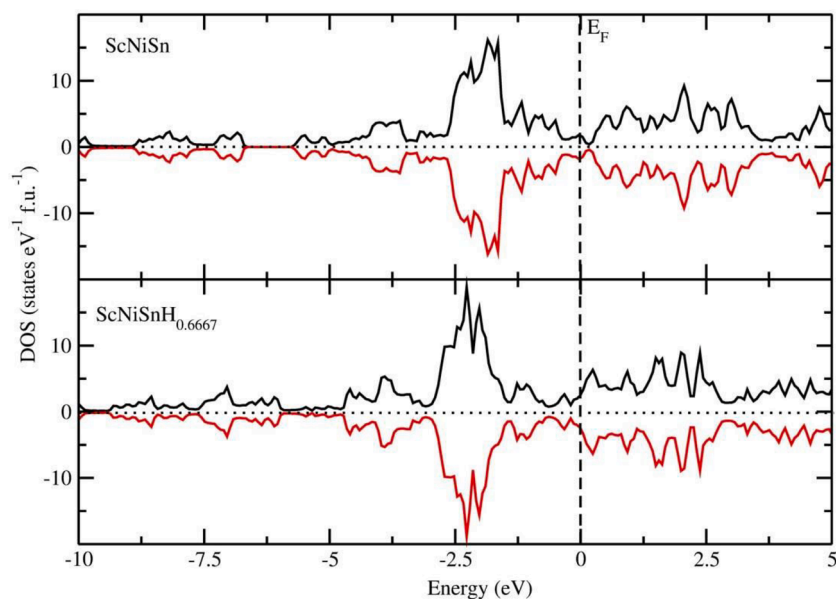


Fig. 9. Calculated total density of states (TDOS) for ScNiSn and its hydride ScNiSnH_{0.667} in sp.gr. $\bar{P}62m$ symmetry.

between -2.8 to -1.9 eV. As the H-*s* and Ni(2)-*d* states are energetically degenerated, this indicates that the interaction between the H and Ni(2) is predominantly covalent.

In order to understand the chemical bonding mechanism in the studied system, we have made valence charge density analyses by making slicing through the different crystal planes for the alloy matrix as well as for the hydrogenated phases. The covalent interaction between Ni and Sn is more probable than ionic interaction as the electronegativity difference between these elements is only 0.05. This was indeed confirmed by the charge density analysis (Fig. 10) which showed that there is a finite electron density present between Ni(1) and Sn. In fact, as will be argued later, the Ni-Sn bond appears to be stronger than the other interatomic bonds in ScNiSn. Ni-Sc and Sn-Sc bonds have a partially mixed covalent-ionic character which may be attributed to the relatively modest electronegativity difference of 0.6 between Sn and Sc and 0.55 between Ni and Sc.

In the ScNiSnH_{0.667} hydride the Ni(2)-H bonds are formed, which are aligned along [001], and these bonds create ...Ni-H-Ni-H... chains; a significant lattice expansion along *c* is a consequence. This rationalizes

the anisotropic changes occurring in the lattice during the hydrogen absorption. A similar type of changes was earlier observed for the LaNiInH_{1.333} hydride [45, 46].

We have made Mulliken population analysis in an attempt to quantify the details of the bonding interactions and to estimate the number of electrons on and between the participating atoms. Although there is no unique definition to identify how many electrons are associated with an atom in a molecule or an atomic grouping in a solid, it has nevertheless proved to be useful in many cases to perform population analyses. Due to its simplicity, the Mulliken population [47] scheme has become the most popular approach. However, this method is more qualitative than quantitative, providing results that are sensitive to the atomic basis. The calculated Mulliken charges are reported in Table 3 for ScNiSn and its hydride ScNiSnH_{0.667}. As a reference point, the commonly recognized nearly pure ionic compound LiH gave Mulliken effective charges (MEC) of $+0.98e$ for Li and $-0.98e$ for H [48]. In the studied compounds the electrons are transferred from Sc and Sn to Ni and H sites. This is evidence of the presence of a partially ionic compound. The calculations show a small charge transfer from Sc to both Ni and H. Such an electron

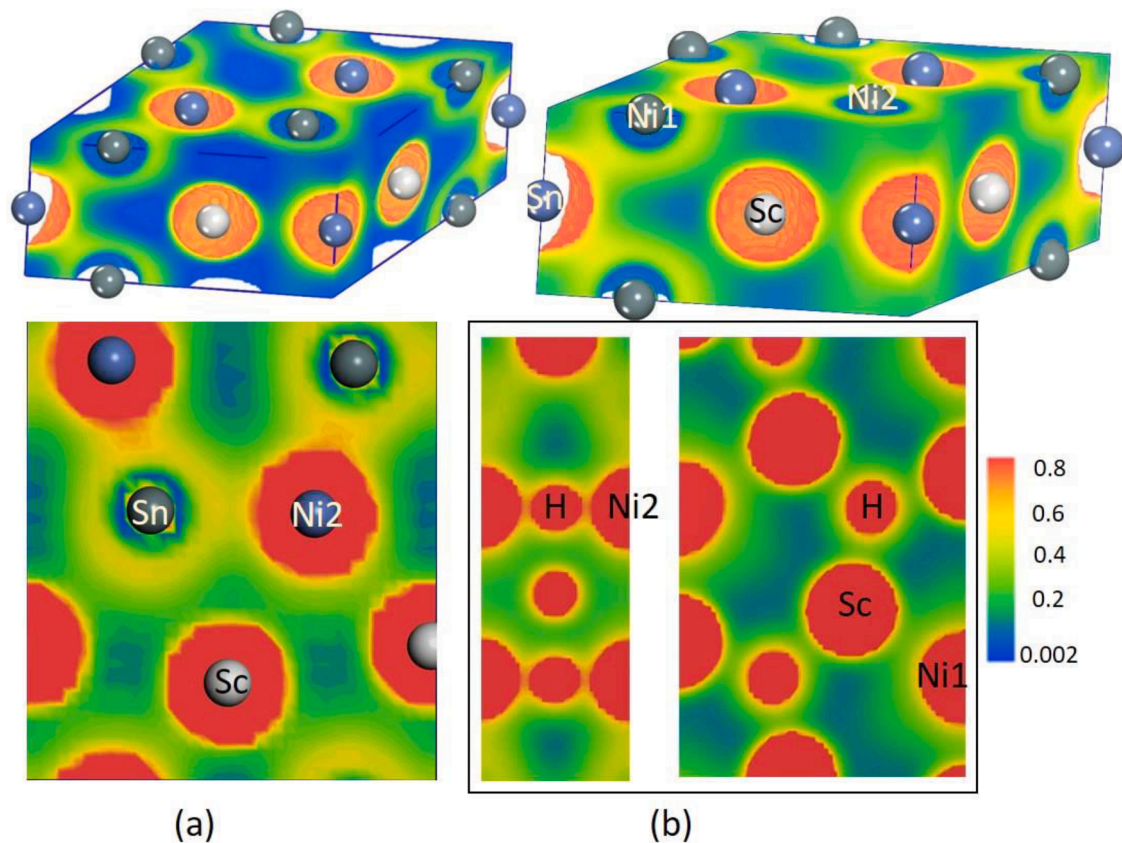


Fig. 10. The valence 3D charge density (upper part) and 2D plots for ScNiSn (a) and its hydride ScNiSnH_{0.667} (b). H-Ni(2) bonding interactions are evident from the figure.

Table 3

Calculated total electrons, Mulliken Population Analysis, Bond Overlap Population (BOP) and interatomic distances for ScNiSn ($P\bar{6}2m$) intermetallic compounds and in its hydride ScNiSnH_{0.667} ($P\bar{6}2m$). The Mulliken-effective charges (MEC) are given in terms of e

	Total e	MEC	BOP	Atomic distance (Å)
ScNiSn				
Sc	10.67	0.33	0.48 (Sc-Ni1) 0.05 (Sc-Ni2) 0.50 (Sc-Sn)	2.848 2.849 2.998
Sn	3.86	0.14	0.79 (Sn-Ni1)	2.6503
Ni(1)	10.55	-0.55	0.22 (Sn-Ni2)	2.6515
Ni(2)	10.43	-0.43		
ScNiSnH_{0.667}				
Sc	10.55	0.45	0.11 (Sc-Ni1) 0.28 (Sc-Ni2)	2.8272 2.8523
Sn	3.79	0.21	0.81 (Sn-Ni1) 0.22 (Sn-Ni2)	2.636 2.6449
Ni(1)	10.60	-0.60		
Ni(2)	10.45	-0.45	0.60 (Ni2-H)	1.844
H	1.24	-0.24	0.10 (H-Sc)	2.176

transfer manifests the formation of a directional bonding between Ni and H that has been observed earlier in our study of the electronic structure of CeNi₃H_{2.7} [49].

Further understanding of the interaction mechanism between the constituents can be obtained from the bond overlap population (BOP) values calculated on the basis of the Mulliken population analysis. The BOP can provide useful information about the hybridization interaction between the constituents. A high BOP value indicates a strong covalent bond, while a low BOP value indicates an ionic interaction. The calculated BOP values for the studied phases are displayed in Table 3. In ScNiSn phase the strongest bonds and their magnitudes line up in the

following sequence Sn-Ni(1) > Sc-Sn > Sc-Ni(1) > Sn-Ni(2) > Sc-Ni(2). When the intermetallic compound is hydrogenated, the strongest Sn-Ni(1) bonding get weakened and the rearranged sequence is Sn-Ni(1) > Ni(2)-H > Sc-Ni(2) > Sn-Ni(2) > Sc-Ni(1) > H-Sc. The strongest (mostly covalent) interactions are Sn-Ni(1) and Ni(2)-H. This finding is well in line with the charge density analysis and electronegativities of the interacting elements.

The optimized atomic positions in the crystal structure of the hydride show that the structural deformation does not lead to any substantial rearrangement of the metal atoms in the basal plane. None of the atoms is significantly shifted in x , y and z coordinates from the ScNiSn. This may be because all atoms are strongly bonded (from the BOP analysis). When H atoms are inserted into the lattice, the atoms of Sc, Ni and Sn rearrange themselves to reach a minimum energy configuration. Hence, the sole possibility to expand the lattice is along the [001] direction. Our charge-density study clearly indicates the formation of ...Ni-H-Ni-H... linear chains along [001], implying an expansion along the c axis. The MEC shows that during the formation of the hydride phase, charges are partially transferred from the electron-rich metal atoms to hydrogen. This may lead to a contraction in the ab plane, hence resulting in the observed lattice deformation upon hydrogenation.

Conclusions

In present work hydrogen interaction with crystallizing with the orthorhombic TiNiSi-type structure ternary intermetallic compound ScNiSn has been studied using hydrogen absorption-desorption characterization, including application of high hydrogen pressures of several GPa H₂, thermal desorption spectroscopy, synchrotron XRD and neutron powder diffraction, together with ¹¹⁹Sn Mössbauer spectroscopy and theoretical DFT calculations of the electronic structures. The hydrogenation of ScNiSn is accompanied by a structural phase transformation

into a hexagonal ZrNiAl-type structure. The formed ScNiSnH_{0.5} hydride displays metallic conductivity, is stable at ambient conditions and completely decomposes on its heating in vacuum releasing hydrogen in a broad temperature range while showing two events of hydrogen release and returning back to the initial TiNiSi-type intermetallic structure. Studies of the crystal structures showed an unusual and quite significant volume contraction on hydrogenation (by -0.8 %) which is associated with rebuilding of the crystal structure and filling by hydrogen atoms in the crystal structure of the ScNiSnD_{0.5} of the trigonal bipyramidal sites Sc₃Ni₂ with interatomic distances of Sc-D=2.1531(6) Å and Ni-D=1.8654(2) Å. High pressure hydrogenation showed that the H storage capacity can be further increased, up to ScNiSnH_{0.83} when performing the hydrogenation at 2 GPa H₂. The high pressure hydride crystallizes with orthorhombic TiNiSi type of structure. Its formation is associated with small volume expansion of 2.04 % and hydrogen insertion into the Sc₃Ni tetrahedral interstices. ¹¹⁹Sn Mössbauer spectroscopy indicated that for the tin site the hydrogenation increases the symmetry from .m. to *m2m* and decreases the isomer shift indicating a slight lowering of the s electron density at tin nuclei. Using generalized gradient-corrected density-functional calculations, the structural stability, electronic structure and bonding in ScNiSn and ScNiSnH_{0.667} were characterized. Our theoretical findings revealed that ScNiSn and ScNiSnH_{0.667} have a finite number of electrons at EF, and thus are classified as metals. Upon the hydrogenation of ScNiSn, the optimized lattice constants exhibit an anisotropic lattice expansion along [001] and a small contraction along [100], in a very good agreement with experimental findings.

In conclusion, scandium even though not being a lanthanide group rare earth metal, closely resembles the behaviors of the heavy lanthanides with H storage behaviors of ScNiSn-based hydride being similar to the HoNiSn-based hydride, where a similar negative expansion effect on the hydrogenation and a formation of a related structure with H atoms filling the Ho₃Ni tetrahedra – a half part of the trigonal bipyramid Ho₃Ni₂ – has been found to occur. Hydrogenation causes a transfer of electronic density from Sc to both Ni and H. Our charge density, MEC and BOP studies show a strong covalent interaction between Ni and H resulting in the directional metal-hydrogen covalent bonding in the ... Ni-H-Ni-H... chains formed in the structure. A strong covalent interaction between Ni and H atoms causes anisotropic lattice deformation along the chains.

Declaration of Competing Interest

The authors declare that they have no known competing financial interests or personal relationships that could have appeared to influence the work reported in this paper.

Acknowledgments

This work received a support from the NATO project G5233 belonging to the Science for Peace and Security Program (VAY and VVB).

The authors appreciate the possibility to collect NPD data at the high-resolution powder diffractometer SPODI at FRMII, Munich, Germany.

PV gratefully acknowledge the Research Council of Norway for providing the computer time (under the project number NN2875k and NS2875k) at the Norwegian supercomputer facility.

Supplementary materials

Supplementary material associated with this article can be found, in the online version, at [doi:10.1016/j.actamat.2022.118549](https://doi.org/10.1016/j.actamat.2022.118549).

References

- [1] V.A. Yartys, T. Olavesen, B.C. Hauback, H. Fjellvåg, H.W. Brinks, Hexagonal LaNiSnD₂ with filled ZrBeSi-type structure, *J. Alloys Compd.* 330-332 (2002) 141–145.
- [2] T. Spataru, P. Palade, G. Principi, P. Blaha, K. Schwarz, V. Kuncser, S. Lo Russo, S. Dal Toé, V.A. Yartys, The nature of the hydrogen bond in the LaNiSnH₂ and NdNiSnH hydrides, *J. Chem. Phys.* 122 (2005), 124703-1-124703-7.
- [3] V.A. Yartys, T. Olavesen, B.C. Hauback, H. Fjellvåg, Orthorhombic NdNiSnD with filled TiNiSi-type structure, *J. Alloys Compd.* 336 (2002) 181–186.
- [4] A. Szytula, O. Isnard, V.A. Yartys, A.B. Riabov, Crystal and magnetic structure of HoNiSnD_{0.67}, *J. Alloys Compd.* 404-406 (2005) 200–203.
- [5] A. Jezierski, A. Szajek, M. Jurczyk, Effect of hydrogenation on the electronic structure of HoNiSn — Ab initio calculations, *Acta Physica Polonica A* 118 (2010) 346–349.
- [6] V.A. Yartys, B. Ouladdiaf, O. Isnard, O.Yu. Khyzhun, K.H.J. Buschow, Hydrogen induced antiferromagnetism in the Kondo semimetal CeNiSn, *J. Alloys Compd.* 359 (2003) 62–65.
- [7] B. Chevalier, J.-L. Bobet, M. Pasturel, E. Bauer, F. Weill, R. Decourt, J. Etourneau, Ferromagnetic behavior of the new hydride CeNiSnH_{1.8(2)}}, *Chemistry of Materials* 15 (2003) 2181–2185.
- [8] T. Spataru, G. Principi, V. Kuncser, W. Keune, V.A. Yartys, Mössbauer study of the RENiSnD (RE: Pr, Nd) monodeuterides, *J. Alloys Compd.* 366 (2004) 81–85, and V. A. Yartys, unpublished results.
- [9] V.A. Yartys, R.V. Denys, O. Isnard, R.G. Delaplane, P. Svedlindh, K.H.J. Buschow, Crystal and magnetic structure of TbNiSnD studied by neutron powder diffraction, *J. Magnet. Magnet. Mater.* 311 (2007) 639–643.
- [10] V.A. Yartys, R.V. Denys, B.C. Hauback, H. Fjellvåg, I.I. Bulyk, A.B. Riabov, Ya. M. Kalychak, Short hydrogen-hydrogen separations in novel intermetallic hydrides, RE₃Ni₃In₃D₄ (RE= La, Ce and Nd), *J. Alloys Compd.* 330-332 (2002) 132–140.
- [11] V.A. Derkach, B.Ya. Kotur, Ternary system Sc-Co(Ni)-Sn at 600°C, in: Abstracts of the 6th International Conference Crystal Chem. Internet. Compd. (Lviv, Ukraine), Lviv, 1995, p. 28.
- [12] V.A. Derkach, B.Ya. Kotur, Yu.K. Gorenlenko, R.V. Skolozdra, Magnetic properties of ScCo₂Sn-ScCoSn alloys, *Inorg. Mater.* 33 (1997) 685–687.
- [13] B.Ya. Kotur, I.P. Klyuchka, New ternary stannides of scandium and cobalt (nickel copper), *Inorg. Mater.* 25 (1989) 518–520.
- [14] R. Mishra, R. Pöttgen, R.-D. Hoffmann, H. Trill, B.D. Mosel, H. Piotrowski, M. F. Zumdick, The stannides RERhSn (RE = Ho - Yb) and ScTSn (T = Pd, Pt) – Structure refinements and ¹¹⁹Sn Mössbauer spectroscopy, *Z. Naturforsch.* 56b (2001) 589–597.
- [15] T. Harmening, C.P. Sebastian, L. Zhang, C. Fehse, H. Eckert, R.A. Pöttgen, ¹¹⁹Sn Mössbauer and ⁴⁵Sc solid state NMR spectroscopic study of the stannides ScTSn (T = Ni, Pd, Pt), *Solid State Sci.* 10 (2008) 1395–1400.
- [16] C.P. Sebastian, L. Zhang, C. Fehse, R.-D. Hoffmann, H. Eckert, R. Pöttgen, New stannide ScAgSn: determination of the superstructure via two-dimensional ⁴⁵Sc solid state NMR, *Inorganic Chemistry* 46 (2007) 771–779.
- [17] V.V. Burnasheva, A.V. Ivanov, V.A. Yartys, K.N. Semenenko, Hydride phases based on scandium-containing intermetallics with the structure of Laves phases, *Inorg. Mater.* 17 (1981) 704–707.
- [18] M. Yoshida, E. Akiba, Hydrogen absorbing properties of ScM₂ Laves phase alloys (M= Fe, Co and Ni), *J. Alloys Compd.* 226 (1995) 75–80.
- [19] W.H. Li, B.H. Tian, P. Ma, E.D. Wu, Hydrogen storage properties of ScMn₂ alloy, *Acta Metall. Sin.* 48 (2012) 822–829.
- [20] W.B. Pearson, *The Crystal Chemistry and Physics of Metals and Alloys*, Wiley-Interscience, New York, 1972.
- [21] M. Hoelzel, A. Senyshyn, N. Juenke, H. Boysen, W. Schmahl, H. Fuess, High-resolution neutron powder diffractometer SPODI at research reactor FRM II, *Nucl. Instrum. Methods Phys. Res. Sect. A: Accelerat., Spectrom., Detect. Assoc. Equip.* 667 (2012) 32–37.
- [22] M. Frontzek, R.E. Whitfield, K.M. Andrews, A.B. Jones, M. Brobek, K. Vodopivec, B. C. Chakoumakos, J.A. Fernandez-Baca, WAND²—A versatile wide angle neutron powder/single crystal diffractometer, *Rev. Sci. Instrum.* 89 (9) (2018), 092801.
- [23] L. Akselrud, Y. Grin, WinCSD: software package for crystallographic calculations (Version 4), *J. Appl. Cryst.* 47 (2014) 803–805.
- [24] L.G. Khvostantsev, V.N. Slesarev, V.V. Brazhkin, Toroid type high-pressure device: history and prospects, *High Pressure Research* 24 (2004) 371–383.
- [25] V.E. Antonov, B.M. Bulychev, V.K. Fedotov, D.I. Kapustin, V.I. Kulakov, I.A. Sholin, NH₃BH₃ as an internal hydrogen source for high pressure experiments, *Int. J. Hydrog. Energy* 42 (2017) 22454–22459.
- [26] I.O. Bashkin, V.E. Antonov, A.V. Bazhenov, I.K. Bdkin, D.N. Borisenko, E. P. Krinichnaya, A.P. Moravsky, A.I. Harkunov, Y.M. Shul'ga, Y.A. Ossipyan, E. G. Ponyatovsky, Thermally stable hydrogen compounds obtained under high pressure on the basis of carbon nanotubes and nanofibers, *JETP Lett.* 79 (2004) 226–230.
- [27] V.J. Long, T.E. Cranshaw, G. Longworth, The ideal Mössbauer effect absorber thickness, *Mössbauer effect reference and data journal* 6 (1983) 42–49.
- [28] R.A. Brand, WinNormos for Igor6, Version for Igor 6.2 or above: 22.02.2017, Universität Duisburg, Duisburg, Germany, 2017.
- [29] G. Kresse, J. Furthmüller, Efficient iterative schemes for ab initio total-energy calculations using a plane-wave basis set, *Phys. Rev. B* 54 (1996) 11169–11186.
- [30] G. Kresse, J. Furthmüller, Efficiency of ab-initio total energy calculations for metals and semiconductors using a plane-wave basis set, *Computat. Mater. Sci.* 6 (1996) 15–50.

- [31] J.P. Perdew, K. Burke, M. Ernzerhof, Generalized gradient approximation made simple, *Phys. Rev. Lett.* 77 (1996) 3865–3868.
- [32] **Materials Data on ScNi₂Sn by Materials Project, United States, 2020**, <https://doi.org/10.17188/1208238>.
- [33] J.F. Riecken, G. Heymann, W. Hermes, U.Ch. Rodewald, R.-D. Hoffmann, H. Huppertz, R. Pöttgen, High-pressure high-temperature studies on the stannides RENiSn (RE = Ce, Pr, Nd, Sm) and REPdSn (RE = La, Pr, Nd), *Z. Naturforsch* 63b (2008) 695–706.
- [34] G. Heymann, B. Heying, U.Ch. Rodewald, O. Janka, H. Huppertz, R. Pöttgen, High-pressure high-temperature crystal growth of equiatomic rare earth stannides RENiSn and REPdSn, *J. Solid State Chem.* 236 (2016) 138–146.
- [35] V.A. Yartys, V.V. Burnasheva, N.V. Fadeeva, V.A. Sarin, L.E. Fykin, K. N. Semenenko, The crystal and magnetic structure of the deuteride ScFe₂D_{2.9}, *Russ. J. Inorg. Chem.* 31 (1986) 175–179.
- [36] V.A. Yartys, V.V. Burnasheva, N.V. Fadeeva, V.A. Sarin, L.E. Fykin, K. N. Semenenko, A neutron diffraction study of the deuteride λ₁-ScFe₂D_{2.5}, *Russ. J. Inorg. Chem.* 31 (1986) 1443–1446.
- [37] V.V. Burnasheva, V.A. Yartys, N.V. Fadeeva, S.P. Solov'ev, K.N. Semenenko, A neutron diffraction study of the deuteride LaNiD_{3.7}, *Russ. J. Inorg. Chem.* 27 (1982) 625–627.
- [38] T. Harmening, C.P. Sebastian, L. Zhang, C. Fehse, H. Eckert, R. Pöttgen, A ¹¹⁹Sn Mössbauer and ⁴⁵Sc solid state NMR spectroscopic study of the stannides ScT₂Sn (T = Ni, Pd, Pt), *Solid State Sci.* 10 (2008) 1395–1400.
- [39] R. Pöttgen, Stannides and intermetallic tin compounds – Fundamentals and applications, *Z. Naturforsch.* 61b (2006) 677–698.
- [40] P.E. Lippens, Interpretation of the Mössbauer isomer shifts in complex tin chalcogenides, *Phys. Rev. B.* 60 (1999) 4576–4586.
- [41] B. Chevalier, C.P. Sebastian, R. Pöttgen, Hydrogenation of the intermediate valence ternary stannides CeRhSn and CeIrSn, *Solid State Sci* 8 (2006) 1000–1008.
- [42] B. Chevalier, R. Decourt, B. Heying, F.M. Schappacher, U.Ch. Rodewald, R. Pöttgen R.-D.Hoffmann, R. Eger, A. Simon, Inducing magnetism in the Kondo semiconductor CeRhSb through hydrogenation: antiferromagnetic behavior of the new hydride CeRhSbH_{0.2}, *Chem. Mater.* 19 (2007) 28–35.
- [43] N.C. Gresty, Y. Takabayashi, A.Y. Ganin, M.T. McDonald, J.B. Claridge, D. Giap, Y. Mizuguchi, Y. Takano, T. Kagayama, Y. Ohishi, M. Takata, M.J. Rosseinsky, S. Margadonna, K. Prassides, Structural Phase Transitions and Superconductivity in Fe_{1+δ}Se_{0.57}Te_{0.43} at Ambient and Elevated Pressures, *J. Am. Chem. Soc.* 131 (2009) 16944–16952.
- [44] M. Krishnan, M. Sathiskumar, K. Ishigaki, J. Gouchi, R. Sankar, Y. Uwatoko, P. Vajeeston, S. Arumugam, *Phys. Rev. B.* (2022) in preparation.
- [45] P. Vajeeston, P. Ravindran, R. Vidya, A. Kjekshus, H. Fjellvåg, V.A. Yartys, Short hydrogen-hydrogen separation in RNiInH_{1.333} (R= La, Ce, Nd), *Phys. Rev. B.* 67 (2003), 014101.
- [46] V.A. Yartys, R.V. Denys, B.C. Hauback, H. Fjellvåg, I.I. Bulyk, A.B. Riabov, Ya. M. Kalychak, Short hydrogen-hydrogen separations in novel intermetallic hydrides, RE₃Ni₃In₃D₄ (RE= La, Ce and Nd), *J. Alloys Compd.* 330-332 (2002) 132–140.
- [47] R.S. Mulliken, Electronic population analysis on LCAO–MO molecular wave functions. I, *J. Chem. Phys.* 23 (1955) 1833–1840.
- [48] P. Vajeeston, P. Ravindran, H. Fjellvåg, Phonon, IR, and Raman spectra, NMR parameters, and elastic constant calculations for AlH₃ polymorphs, *J. Phys. Chem. A* 115 (2011) 10708–10719.
- [49] V.A. Yartys, P. Vajeeston, A.B. Riabov, P. Ravindran, R.V. Denys, J.P. Maehlen, R. G. Delaplane, H. Fjellvåg, Crystal chemistry and metal-hydrogen bonding in anisotropic and interstitial hydrides of intermetallics of rare earth (R) and transition metals (T), RT₃ and R₂T₇, *Z. Kristallogr.* 223 (2008) 674–689.